Death of Massive Stars: Supernovae and Gamma-Ray Bursts
Proceedings IAU Symposium No. 279, 2012
P. Roming, N. Kawai & E. Pian, eds.

doi:10.1017/S1743921312012847

3D Core-Collapse Supernova Simulations: Neutron Star Kicks and Nickel Distribution

Annop Wongwathanarat, Hans-Thomas Janka, and Ewald Müller

Max-Planck Institut für Astrophysik, Karl-Schwarzschild-Straße 1, D-85748 Garching, Germany
email: annop@mpa-garching.mpg.de

Abstract. We perform a set of neutrino-driven core-collapse supernova (CCSN) simulations studying the hydrodynamical neutron star kick mechanism in three-dimensions. Our simulations produce neutron star (NS) kick velocities in a range between ∼100-600 km/s resulting mainly from the anisotropic gravitational tug by the asymmetric mass distribution behind the supernova shock. This stochastic kick mechanism suggests that a NS kick velocity of more than 1000 km/s may as well be possible. An enhanced production of heavy elements in the direction roughly opposite to the NS recoil direction is also observed as a result of the asymmetric explosion. This large scale asymmetry might be detectable and can be used to constrain the NS kick mechanism.

Keywords. (stars:) supernovae: general, (stars:) pulsars: general

1. Introduction

Observations of young pulsars show that they possess space velocities approximately 250-400 km/s on average (Hobbs *et al.* 2005; Faucher-Giguère & Kaspi 2006). Even velocities beyond 1000 km/s, which are much larger than the velocity of SN progenitor stars, are observed (Chatterjee *et al.* 2005). Therefore, two possibilities exist for the mechanism to produce these high NS velocities. Either the NS acquires its velocity at the time of its birth during the SN explosion or it gradually builds up its velocity at a later time (see, *e.g.,* Lai *et al.* 2001 for review). We aim to investigate one of the proposed mechanisms, namely the hydrodynamically driven kick mechanism, to answer the question whether or not this mechanism can produce large NS recoil velocities. While simulations in two spatial dimensions have been performed by Scheck *et al.* (2004,2006) and Nordhaus *et al.* (2010,2011), Wongwathanarat *et al.* (2010b) performed a small set of 3D simulations for the first time. Here, we extend our previous study by considering a larger set of parameters.

2. Numerical methods

All simulations are performed with the explicit finite-volume Eulerian multi-fluid hydrodynamics code Prometheus (Fryxell *et al.* 1991; Müller *et al.* 1991a,b). The multi-dimensional hydrodynamic equations are solved in spherical polar coordinates using the dimensional splitting method of Strang (1968), the piecewise parabolic reconstruction scheme (Colella & Woodward 1984), and a Riemann solver for real gases (Colella & Glaz 1985). The AUSM+ fluxes of Liou (1996) are used to replace the fluxes computed by the Riemann solver inside grid cells with strong grid-aligned shocks to prevent odd-even decoupling (Quirk 1994). Advection of nuclear species is treated by the Consistent Multi-fluid Advection (CMA) scheme as described in Plewa & Müller (1999).

2.1. *Initial models and additional physics*

We considered three different non-rotating SN progenitor models: a $15\,M_\odot$ progenitor, s15s7b2 of Woosley & Weaver (1995), a $15\,M_\odot$ star evolved by Limongi *et al.* (2000), and a $20\,M_\odot$ progenitor star for SN1987A developed by Shigeyama & Nomoto (1990). In the following, these models are called W15, L15, and N20, respectively. These progenitors are evolved through collapse and core bounce in one dimension using the PROMETHEUS-VERTEX code, which includes an energy-dependent neutrino transport solver (A. Marek and R. Buras, private communication). Our simulations then started from the 1D output data at approximately 15 ms after the core bounce. To break the spherical symmetry, random seed perturbations of 0.1% amplitude are imposed on the radial velocity field since our code otherwise preserves exact spherical symmetry of the initial state.

The SN explosion is initiated by imposing a suitable neutrino luminosity at the inner grid boundary. The volume inside the inner grid boundary contains the innermost $\sim 1.1\,M_\odot$ of the PNS, which are excised and replaced by a point mass situated at the coordinate origin. We apply a simplified grey neutrino transport using the "ray-by-ray" approach following Scheck *et al.* (2006). Newtonian self-gravity of the stellar fluid in 3D is taken into account by solving Poisson's equation in its integral form using the spherical harmonics expansion technique of Müller & Steinmetz (1995). The monopole term is corrected for general relativistic effects as described in Scheck *et al.* (2006) and Arcones *et al.* (2007). We use the subnuclear equation of state of Janka & Müller (1996), and include a small alpha-reaction nuclear network consisting of 13 alpha group nuclei (^{4}He to ^{56}Ni) and a tracer nucleus tracing neutron-rich material as described in Kifonidis *et al.* (2003).

2.2. *Domain discretization and grid setup*

It is well known that discretizing a sphere using the usual spherical polar (or latitude-longitude) grid leads to a severe timestep restriction due to the CFL condition in the polar regions. Therefore, to ease this problem, we employed the "Yin-Yang" overlapping grid technique developed by Kageyama & Sato (2004) for simulations in geophysical science. It consists of two geometrically identical grid patches which contain only the low-latitude part of a spherical polar grid. Thus, when compared to the spherical polar grid, a much larger timestep can be chosen (up to a factor of 40 larger for an angular resolution of 2°). Details regarding the numerical implementation of the Yin-Yang grid for astrophysical self-gravitating systems are given in Wongwathanarat *et al.* (2010a).

Our standard grid configuration consists of $400(r) \times 47(\theta) \times 137(\phi) \times 2$ grid cells corresponding to an angular resolution of 2°. Three simulations denoted with the suffix "lr" are conducted with a lower angular grid resolution of 5° ($400(r) \times 18(\theta) \times 54(\phi) \times 2$ grid cells). The radial grid resolution is kept constant at $\Delta r = 0.3$ km from the inner grid boundary out to a radius of approximately 100 km (depending on the model). Outside of this radius the radial grid is logarithmically spaced. The outer grid boundary R_{ob} is placed sufficiently far out (approximately at 18000 km) to prevent the SN shock wave from leaving the computational grid during the simulated epoch. Hydrostatic equilibrium is assumed at the inner, retracting radial grid boundary R_{ib}, while a free outflow boundary condition is employed at the outer one.

3. Results

We have calculated 15 models in 3D considering three different non-rotating progenitor stars. We varied the neutrino luminosities imposed at the inner grid boundary to obtain explosions with different energies and onset times. Because the development of

https://doi.org/10.1017/S1743921312012847 Published online by Cambridge University Press

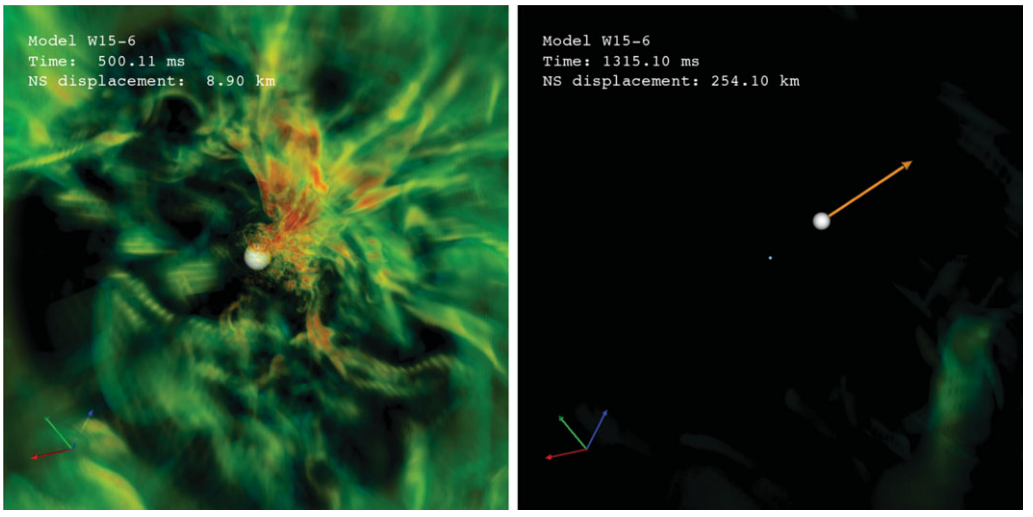

Figure 1. Left: Ejecta asymmetry visualized by a ray-casting technique for model W15-6. A large-scale ($\ell = 1$) asymmetry of the ejecta mass distribution resulting in a large NS kick velocity can clearly be seen shortly after the onset of the explosion. It exhibits the strongest amplitude roughly at $t = 500$ ms after bounce. As shown in the figure, denser clumps (red color) remain close to the NS (white ball) exerting a large gravitational pull towards the upper right direction. Right: The NS and its velocity vector (orange arrow) pointing to the upper right direction shown at the end of the simulation, $t = 1.3$ s after bounce. The displacement of the NS from the coordinate origin (white dot at the center of the figure) is obtained by performing a time-integration of the NS recoil velocity.

hydrodynamic instabilities in our simulations proceeds chaotically, changing only the initial seed perturbation pattern allows us to obtain explosions with morphologically different ejecta asymmetries. Tables summarizing explosion and NS properties obtained from these models can be found in Wongwathanarat *et al.* (2010b) and Wongwathanarat *et al.* (2012).

The NS recoil velocity, $\vec{v}_{ns}$, as a function of time t is calculated by assuming conservation of linear momentum, *i.e.*, $\vec{v}_{ns}(t) = -\vec{P}_{gas}(t)/M_{ns}(t)$, where $\vec{P}_{gas}$ and M_{ns} are the total linear momentum of the ejecta and the NS mass, respectively. We define the NS radius, R_{ns}, to be the radius where the gas density $\rho = 10^{11}$ g/cm^3. From our set of 15 models, we obtain a maximum NS kick velocity of 437 km/s (model W15-6) at 1.3 s after bounce, when the NS is still accelerating with 222 km/s^2. We expect the NS recoil velocity of this model to grow well beyond 600 km/s. This claim is supported by model W15-2 which has a slightly lower velocity at 1.3 s after bounce than model W15-6. Model W15-2 leads to a NS recoil velocity of 575 km/s at 3.3 s after bounce. Following the analysis of Scheck *et al.* (2006), we integrate various hydrodynamical forces acting on the NS to evaluate the contribution by each force to the NS acceleration and find that the gravitational tug is the dominant force. The tug force by asymmetrically distributed dense clumps lagging behind in the ejecta will act for a timescale of a few seconds. Figure 1 shows the large-scale ($\ell = 1$) asymmetry of the mass distribution behind the SN shock for model W15-6. This kick mechanism is different from that where the NS kick velocity originates from many small thrusts of downflow material pushing the NS in random directions (*e.g.*, Spruit & Phinney 1998).

The asymmetric explosion also leads to an asymmetry in the production of heavy elements such as ^{56}Ni. We observe that the SN shock's strength is largest in the direction roughly opposite to the recoil direction of the NS for models which exhibit strong NS

https://doi.org/10.1017/S1743921312012847 Published online by Cambridge University Press

recoils. The SN shock compresses the ejecta to higher temperature in this direction, leading to higher abundances of explosively produced heavy elements. We calculated the total mass of each element contained in each hemisphere using the NS recoil direction as the north pole. It turned out that a clear relative difference between the two hemispheres in the abundances of elements heavier than ^{28}Si can be expected. This relative difference can amount up to 50% in mass. This is different from the result obtained by Fryer & Kusenko (2006) who investigated NS kicks resulting from asymmetric neutrino emission, the so-called neutrino-driven kick. In that case, more heavy elements are predicted in the direction of the NS recoil. Such an asymmetry is likely to be preserved during the later evolution of the explosion, and if observed, it might provide a strong constraint to the NS kick mechanism.

References

Arcones, A., Janka, H., & Scheck, L. 2007, *A&A*, 467, 1227

Chatterjee, S., Vlemmings, W. H. T., Brisken, W. F., Lazio, T. J. W., Cordes, J. M., Goss, W. M., Thorsett, S. E., Fomalont, E. B., Lyne, A. G., & Kramer, M. 2005, *ApJ*, 630, L61

Colella, P. & Glaz, H. M. 1985, *J. Comput. Phys.*, 59, 264

Colella, P. & Woodward, P. R. 1984, *J. Comput. Phys.*, 54, 174

Faucher-Giguère, C. & Kaspi, V. M. 2006 *ApJ*, 643, 332

Fryer, C. L. & Kusenko, A. 2006, *ApJS*, 163, 335

Fryxell, B., Müller, E., & Arnett, D. 1991, *ApJ*, 367, 619

Hobbs, G., Lorimer, D. R., Lyne, A. G., & Kramer, M. 2005, *MNRAS*, 360, 974

Janka, H. & Müller, E. 1996, *A&A*, 306, 167

Kageyama, A. & Sato, T. 2004, *Geochemistry Geophysics Geosystems*, 5

Kifonidis, K., Plewa, T., Janka, H., & Müller, E. 2003, *A&A*, 408, 621

Lai, D., Chernoff, D. F., & Cordes, J. M. 2001, *ApJ*, 549, 1111

Limongi, M., Straniero, O., & Chieffi, A. 2000, *ApJS*, 129, 625

Liou, M.-S. 1996, *J. Comput. Phys.*, 129, 364

Müller, E., Fryxell, B., & Arnett, D. 1991a, *A&A*, 251, 505

Müller, E., Fryxell, B., & Arnett, D. 1991b, in *European Southern Observatory Conference and Workshop Proceedings*, edited by I. J. Danziger & K. Kjaer, vol. 37, 99

Müller, E. & Steinmetz, M. 1995, *Comput. Phys. Commun.*, 89, 45

Nordhaus, J., Brandt, T. D., Burrows, A., Livne, E., & Ott, C. D. 2010, *Phys. Rev. D*, 82, 103016

Nordhaus, J., Brandt, T. D., Burrows, A., & Almgren, A. 2011, arxiv:1112.3342

Plewa, T. & Müller, E. 1999, *A&A*, 342, 179

Quirk, J. J. 1994, *Int. J. Num. Meth. Fluids*, 18, 555

Scheck, L., Kifonidis, K., Janka, H., & Müller, E. 2006, *A&A*, 457, 963

Scheck, L., Plewa, T., Janka, H.-T., Kifonidis, K., & Müller, E. 2004, *Phys. Rev. Lett.*, 92, 011103

Shigeyama, T. & Nomoto, K. 1990, *ApJ*, 360, 242

Spruit, H. & Phinney, E. S. 1998, *Nature*, 393, 139

Strang, G. 1968, *SIAM J. Numer. Anal.*, 5, 506

Wongwathanarat, A., Hammer, N. J., & Müller, E. 2010a, *A&A*, 514, A48

Wongwathanarat, A., Janka, H., & Müller, E. 2010b, *ApJL*, 725, L106

Wongwathanarat, A., Janka, H., & Müller, E. 2012, to be submitted to *A&A*

Woosley, S. E. & Weaver, T. A. 1995, *ApJS*, 101, 181